Compact Multi-Band H-Shaped Slot Antenna

Tze-Hsuan Chang and Jean-Fu Kiang

***Abstract*—A compact triple-band H-shaped slot antenna fed by microstrip coupling is proposed. Four resonant modes are excited, including a monopole mode, a slot mode, and their higher-order modes, to cover GPS (1.575 GHz) and Wi-Fi (2.4–2.485 GHz and 5.15–5.85 GHz), respectively. Sensitivity study of the slot geometry upon the resonant modes have been conducted. The measured gains at these four resonant frequencies are 0.2 dBi, 3.5 dBi, 2.37 dBi, and 3.7 dBi, respectively, and the total efficiencies are −2.5 dB, −1.07 dB, −3.06 dB, and −2.7 dB, respectively. The size of this slot antenna is only $0.24\lambda_0 \times 0.034\lambda_0$, where λ_0 is the free-space wavelength at 1.575 GHz, hence is suitable to install on notebook PC's and handheld devices.**

***Index Terms*—Multiple bands, resonant modes, slot antenna.**

I. Introduction

With the growing demand of positioning, navigation, and WLAN access on mobile phone, antennas on handheld devices are needed to support multiple bands of GPS (1.575 GHz) and Wi-Fi (2.4–2.485 GHz and 5.15–5.85 GHz). Handheld devices are preferred to be thinner, leaving less space to accommodate separate antennas. Moreover, metal casing near conventional antennas, such as monopoles and inverted-F antennas, tend to reduce their bandwidth and radiation efficiency. Hence, slot antennas become attractive for mobile devices, especially for those with metal casing.

The bandwidth of slot antennas can be increased by altering the shapes of the slots, the main radiating elements. Larger slot indicates larger radiating area and a lower Q-factor, which implies a wider bandwidth [1]. With proper design, various structures or shapes of slot antennas have been proposed to achieve a wide bandwidth, including circular shape [2], elliptical shape [3], triangles [4], and fractal [5].

In some cases, the feeding microstrip functions as a monopole antenna, contributing extra bandwidth to the plain slot antennas [6]–[9]. A wide slot may also support more resonant modes, and two nearby resonant modes can be merged to form a wider bandwidth [10], [11]. In [12], a wide-slot antenna is fed by a fork-shaped microstrip line, and the bandwidth can be optimized by tuning the stubs. An L-shaped slot fed by a W-shaped stub has been designed to increase its bandwidth [13]. Adding parasitic elements to the microstrip feed line can serve the same purpose [14]. However, these designs require large area for slot, hence is not suitable for handheld devices.

It is a challenging task to design a small yet wideband slot antenna to cover 1.575 to 5.85 GHz. Multiband slot antenna is an alternative solution, which is usually designed using multiple slots [15]–[18]. In [15], multiple bandwidths are achieved with two independent slots. Two adjacent open-ended slots, also called monopole slots, resonate at $\lambda_g/4$ and exhibit multiple bands [16]. In [17], a combination of E-shaped and T-shaped monopole slots is proposed to achieve multiple bands for GSM/WCDMA/WLAN. In [18], three monopole slots are placed at proximity to provide multiple wide bands for WWAN applications. Adding triangular patch to triangular ring slot antenna has been demonstrated dualband characteristic [19]. These approaches also take a large area or become too complicated to implement on small devices. In [20], a tunable dual-band slot antenna is designed by varying the capacitance of a varactor across the slot.

Several triple-band slot antennas have also been developed. For example, a CPW-fed dipole-like slot antenna is reported to have three nearly uncoupled bands with wide tuning ranges [21]. In [8] and [9], a pair of strips are embedded in the inner edge of the slot to create additional resonance and to interact with the feeding monopole to achieve triple bands. However, the size of these triple-band slot antennas is large if the 1.575 GHz band is to be covered.

In this work, a compact triple-band H-shaped slot antenna is proposed, which can be used for GPS and Wi-Fi applications. Unlike [8] and [9], in which strips are used to create additional resonances, our design combines a narrow-width rectangular slot and a strip monopole to generate four resonant modes, including the fundamental modes of the monopole and the rectangular slot, as well as their high-order modes. These resonant modes will be highlighted by their current or electric field distributions. Simulations are conducted to better understand the antenna behavior, to tune their resonant frequencies, and to optimize the bandwidth. The radiation patterns and antenna efficiencies are also presented.

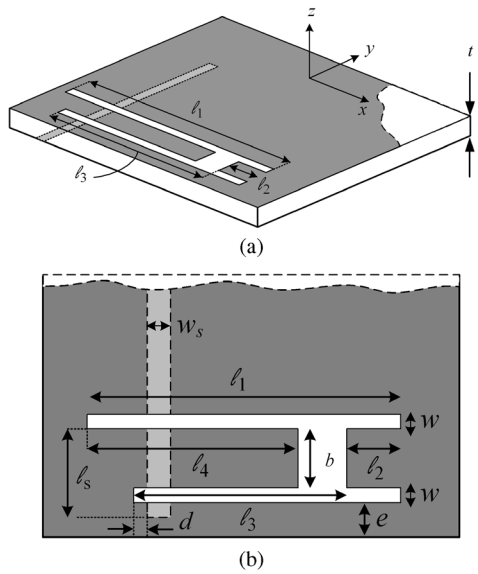

Fig. 1. Configuration of H-shaped slot antenna fed by microstrip coupling. The ground size is $60 \times 60\ \mathrm{mm}^2$, and the distance from slot to edge is $e = 3.5\ \mathrm{mm}$, (a) panoramic view, (b) top view.

II. Antenna Configuration

Fig. 1 depicts the configuration of the H-shaped slot antenna, which is fabricated on an FR4 substrate ($\epsilon_r = 4.5$, $\tan\delta = 0.025$) of thickness $t = 0.7\ \mathrm{mm}$ and 60 mm × 60 mm in size, coated with copper on one side. The H-shaped slot can be viewed as a wide aperture of size $\ell_1 \times (2w + b)$, inserted with two metal strips of dimensions $\ell_2 \times b$ and $\ell_4 \times b$, respectively, leaving two slots of width w on both edges of the aperture. A 50 Ω microstrip line of width $w_s = 1.1\ \mathrm{mm}$ is printed on the opposite side to the ground plane on which the H-shaped slot is carved, to couple energy to the slot antenna.

Manuscript received December 16, 2012; revised March 16, 2013; accepted April 20, 2013. Date of publication May 13, 2013; date of current version July 31, 2013. This work was supported in part by Foxconn and in part by the National Science Council, Taiwan, ROC, under contract NSC 100-2221-E-002-232.

T.-H. Chang was with the Graduate Institute of Communication Engineering, National Taiwan University, Taipei, Taiwan. He is now with Foxconn, Shenzhen City, Guangdong Province, China.

J.-F. Kiang is with the Department of Electrical Engineering and the Graduate Institute of Communication Engineering, National Taiwan University, Taipei, Taiwan (e-mail: jfkiang@cc.ee.ntu.edu.tw).

Digital Object Identifier 10.1109/TAP.2013.2262666

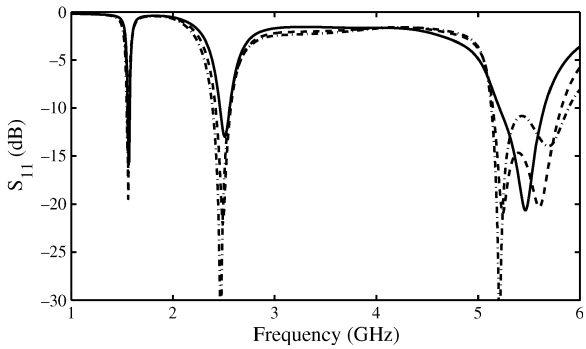

Fig. 2. Effects of microstrip offset d on reflection coefficient, $\ell_1 = 45.5$ mm, $\ell_2 = 5$ mm, $\ell_3 = 36$ mm, $\ell_4 = 34.5$ mm, $w = 1.5$ mm, $\ell_s = 6.5$ mm, and $b = 3.5$ mm, ——: $d = -1$ mm, – – –: $d = 0$ mm, –·–: $d = 0.5$ mm.

By properly tuning different parts of the slot, different modes of the strip monopoles and the slot arms can be adjusted to resonate at the desired frequencies. These modes can be excited simultaneously, and the microstrip position d and length ℓ_s can be optimized to achieve a wide impedance bandwidth. By simulation, it is found that the optimal microstrip length ℓ_s is longer than $b+w$, and the parameter d is greater than zero to obtain a wider bandwidth over the 5.15–5.85 GHz band.

Fig. 2 shows the effect of microstrip position, d, on the input impedance and resonant frequencies. Four distinctive resonant frequencies are observed at 1.575, 2.5, 5.2 and 5.8 GHz when $d = 0.5$ mm. As d is increased, the first resonant frequency is hardly affected, while the second resonant frequency near 2.5 GHz slightly decreases, because the current path surrounding the slot becomes longer. Note that the 10-dB impedance bandwidth over 5.15–5.85 GHz is contributed by the third and the fourth modes. When d is gradually decreased from 0.5 to 0 mm, the third and the fourth resonant frequencies move closer to each other, and finally merge when $d = -1$ mm, causing a bandwidth reduction. By properly adjusting feeding position, the bandwidth over 5–6 GHz can be achieved.

Simulation shows that the slot-to-edge distance, e, does not significantly affect the resonant frequencies as e is increased from 1.5 mm to 5.5 mm. However, the 10-dB impedance bandwidth of the fundamental slot mode is increased and its total antenna efficiency is improved by about 0.4 dB. On the other hand, the total antenna efficiency of the third-harmonic mode of the strip monopole is reduced by about 0.8 dB. As a trade-off, $e = 3.5$ mm is chosen.

III. Resonance Mechanisms

To further analyze the resonance behavior shown in Fig. 2, the current distribution on the inserted strips and the electric field distribution on the slot arms are observed to explain their behaviors. Fig. 3(a) shows the current distribution on the left strip of dimensions $\ell_4 \times b$, connected to the ground plane on the left edge of the aperture. The left strip resonates at 1.575 GHz, like a monopole antenna at its fundamental mode. The strip is surrounded closely by the ground, over a slot of width w, incurring strong capacitive effect. Hence, its resonant frequency and bandwidth are reduced.

Fig. 3(b) depicts the current distribution on the strip, of a higher-order mode at 5.2 GHz. It is a standing wave of one and a half guided wavelength along the strip. The resonant frequencies are mainly determined by the length ℓ_4, and slightly affected by w which is related to a capacitive loading.

The H-shaped slot can be viewed as a rectangular aperture of dimensions $\ell_1 \times (b + 2w)$, perturbed by two strips of dimensions $\ell_4 \times b$ and

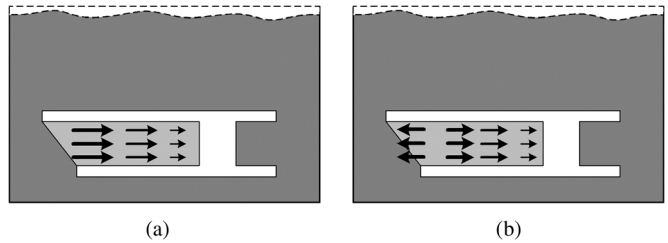

Fig. 3. Current distributions on the strip area of dimension $\ell_4 \times b$, (a) fundamental mode at 1.575 GHz ($\ell_4 = \lambda_g/2$), (b) third-harmonic mode at 5.2 GHz ($\ell_4 = 3\lambda_g/2$), where λ_g is guided wavelength along the strip.

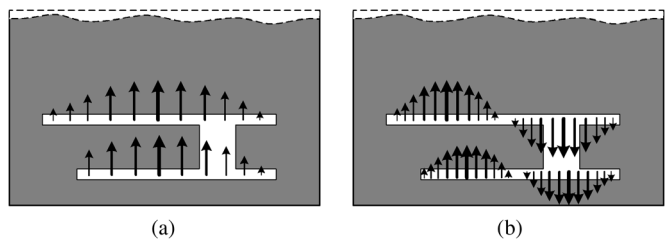

Fig. 4. Electric field distribution on the slot, (a) first resonant mode of the slot at 2.5 GHz, (b) second resonant mode of the slot at 5.6 GHz.

$\ell_2 \times b$, respectively. Fed by the offset microstrip coupling, two resonant slot modes are excited at 2.5 GHz and 5.6 GHz, respectively, as shown in Fig. 2 with $d = 0.5$ mm.

For the resonant mode at 2.5 GHz, a small portion of surface current flows into the two strips of lengths ℓ_2 and ℓ_4, respectively; and most of the surface current flows around the outer contour of the H-shaped slot. As depicted in Fig. 4(a), the electric field distribution has a half-wavelength sinusoidal form, which is the fundamental mode of a slot. Since $\ell_1 \geq \ell_3 + \ell_2$, the resonant frequency is primarily determined by ℓ_1, with minor effect from the width $b + 2w$.

Fig. 4(b) shows the second resonant mode of the slot, with the resonant frequency resonant frequency of 5.6 GHz. The electric field distribution within the slot is a one-wavelength sinusoidal. The surface current flows along the edges of the inserted strips, with lengths of ℓ_2 and ℓ_4, respectively. The complete current path is shorter than the path length measured along the center of the slots, making the resonant frequency higher than twice of the fundamental frequency. Since the resonant frequencies of the third-harmonic along the strip-monopole and the second resonant mode of the slot are close, their fields interact with each other, making their associated bandwidths sensitive to the geometrical dimensions and the feeding structure.

IV. Sensitivity Analysis on Parameters

Variation of the key geometrical parameters, ℓ_1, ℓ_2, ℓ_3 and ℓ_4, on the resonant frequencies is studied by simulation using HFSS. Each parameter is varied while keep the others the same.

A. Effect of ℓ_1

The fundamental mode of the slot arm at 2.5 GHz is primarily determined by ℓ_1. As shown in Fig. 5, when the slot length ℓ_1 is increased from 44 to 46 mm, the resonant frequency decreases from 2.54 to 2.45 GHz. Also, as ℓ_1 is increased, the distance between the two inserted strips with lengths ℓ_4 and ℓ_2 increases as well, thus reducing the capacitive loading on the two strip monopoles. As a consequence, the fundamental and the third-harmonic resonant frequencies of the monopole increase from 1.54 to 1.56 GHz and from 4.96 to 5.28 GHz, respectively. The second resonant mode of the slot arms at 5.6 GHz is slightly affected.

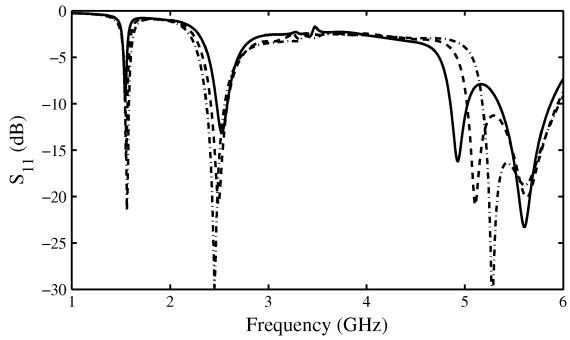

Fig. 5. Effect of slot dimension ℓ_1, all parameters are the same as in Fig. 2 with $d = 0.5$ mm, ——: $\ell_1 = 44$ mm, – – –: $\ell_1 = 45$ mm, –·–: $\ell_1 = 46$ mm.

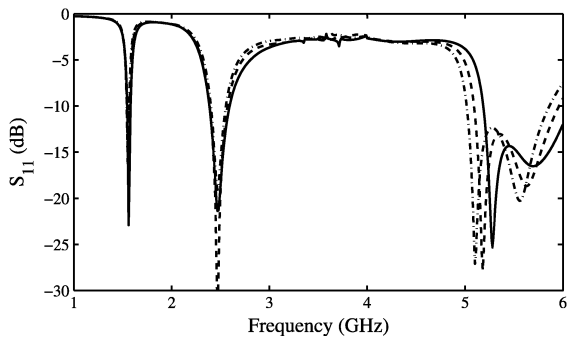

Fig. 6. Effect of strip length ℓ_2, all parameters are the same as in Fig. 2 with $d = 0.5$ mm, ——: $\ell_2 = 4.5$ mm, – – –: $\ell_2 = 5$ mm, –·–: $\ell_2 = 5.5$ mm.

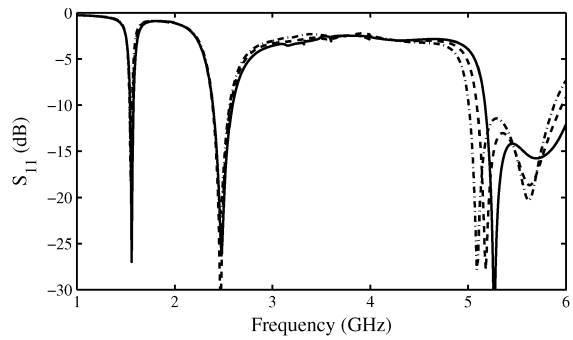

Fig. 7. Effect of slot dimension ℓ_3, all parameters are the same as in Fig. 2 with $d = 0.5$ mm, ——: $\ell_3 = 35.5$ mm, – – –: $\ell_3 = 36$ mm, –·–: $\ell_3 = 36.5$ mm.

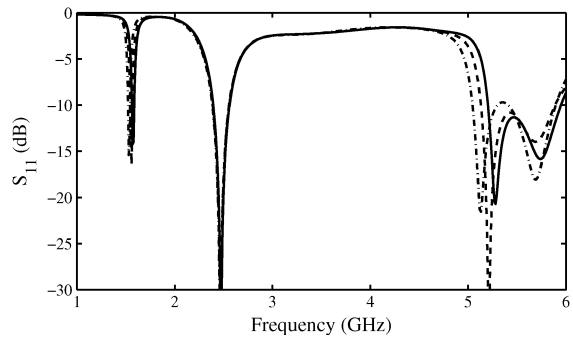

Fig. 8. Effect of strip length ℓ_4, all parameters are the same as in Fig. 2 with $d = 0.5$ mm, ——: $\ell_4 = 34$ mm, – – –: $\ell_4 = 34.5$ mm, –·–: $\ell_4 = 35$ mm.

B. Effect of ℓ_2

Fig. 6 shows that as ℓ_2 increases from 4.5 to 5.5 mm, the separation between the two strips of lengths ℓ_4 and ℓ_2 is reduced, leading to a larger capacitive loading to both strip-monopoles. Hence, the fundamental and the third-harmonic resonant frequencies of the strip-monopoles is decreased from 1.57 to 1.55 GHz and from 5.28 to 5.09 GHz, respectively. In addition, the periphery around the slot is also increased as ℓ_2 increases, hence the second resonant frequency of the slot arms is decreased from 5.7 to 5.56 GHz. Also note that the bandwidth of the slot mode is slightly reduced when ℓ_2 increases because of its reduced radiating aperture area.

C. Effect of ℓ_3

Fig. 7 shows the effect of ℓ_3 on the resonant frequencies. The fundamental mode of the strip-monopoles is not affected by ℓ_3; instead it is mainly determined by ℓ_4. Because $\ell_1 \geq \ell_2 + \ell_3$, the fundamental mode of the slot arms is strongly affected by ℓ_1 rather than ℓ_3. The outer periphery of the slot is lengthened as ℓ_3 is increased, rendering the second resonant frequency of the slot reduced from 5.6 GHz. On the other hand, the third-harmonic resonant frequency of the strip-monopoles is inversely proportional to the effective length of the monopole. It is observed that the higher-order mode is more sensitive to the antenna dimensions than the fundamental mode.

D. Effect of ℓ_4

When the strip length ℓ_4 is increased, the resonant frequencies of the fundamental and the third-harmonic of the strip-monopoles are decreased, as shown in Fig. 8. The resonant frequencies of the slot modes are rarely affected, and only the input impedance of the second slot mode, at 5.6 GHz, is affected.

In summary, the lengths ℓ_1 and ℓ_4 can be tuned to adjust the lowest two resonant frequencies. Usually, the fundamental strip-monopole mode has a narrow bandwidth, but is sufficient to cover GPS applications. The bandwidth of the first slot mode can be widened by increasing the slot area, for example, by increasing the width w. The two higher bands can be fine-tuned with ℓ_2 and the microstrip position d to merge the bands of the third-harmonic mode of the strip-monopole and the second slot mode. The 10-dB impedance bandwidth can be optimized to cover 5.15–5.825 GHz.

V. Final Design and Radiation Patterns

A prototype H-shaped slot antenna is fabricated to verify the simulated results of both the input impedance and the radiation characteristics. Fig. 9 shows the reflection coefficient of this H-shaped slot antenna. The measurement results match the simulation results reasonably well, the deviation may be caused by fabrication tolerance. Four resonant modes are excited as expected. Its 10-dB bandwidths cover 1.555–1.5775 GHz (1.5%), 2.395–2.695 GHz (12%), and 4.975–5.935 GHz (17%); ready for GPS and Wi-Fi applications.

Fig. 10 shows the radiation patterns at 1.575 GHz. The measurement and simulation results match reasonably well. The current on the strip and the ground mainly flows in the $\hat{x}$ direction. The electric field on the slots has z and y components, accounting for the E_ϕ and E_θ components of the radiation patterns. The E_ϕ component on the xz-plane is nearly omnidirectional, with variations within 3 dB. Note that the strip monopole is surrounded by the ground, its gain is about 0.2 dBi at 1.575 GHz; and the peak gain is 0.26 dBi, at 1.565 GHz.

Fig. 11 shows the radiation patterns at 2.5 GHz. Again, the measurement and simulation results match fairly well. The measured antenna gain is about 3.5 dBi. The radiation patterns are contributed by the slot arms laid on the xy-plane with strong E_y component. The E_ϕ pattern

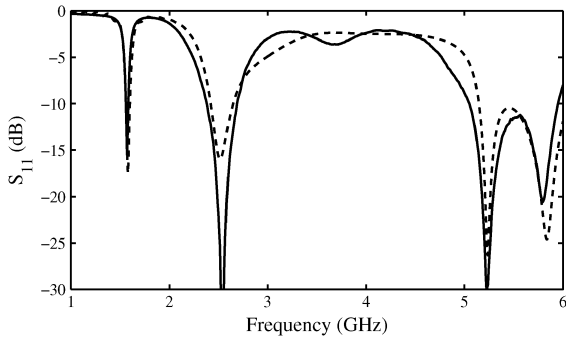

Fig. 9. Measured and simulated reflection coefficients, $\ell_1 = 46$ mm, $\ell_2 = 4.8$ mm, $\ell_3 = 36.7$ mm, $\ell_4 = 35$ mm, $w = 1.9$ mm, $\ell_s = 6.5$ mm, $d = 0.5$ mm, and $b = 3$ mm, ——: measurement, − − −: simulation.

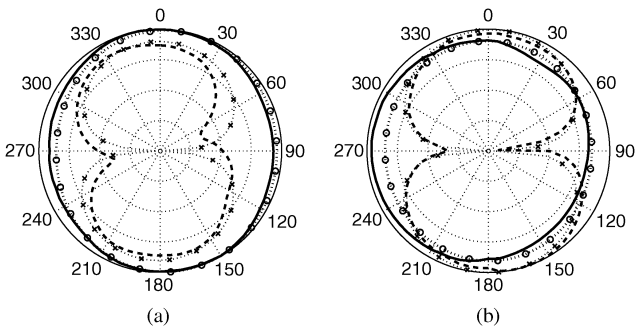

Fig. 10. Radiation patterns at 1.575 GHz, (a) xz-plane, (b) yz-plane, ——: measured E_ϕ, − − −: measured E_θ, $\cdots\circ\cdots$: simulated E_ϕ, $-\cdot\times-\cdot$: simulated E_θ, all parameters are the same as in Fig. 9.

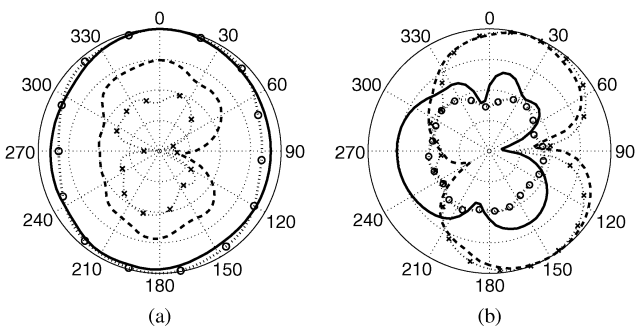

Fig. 11. Radiation patterns at 2.5 GHz, (a) xz-plane, (b) yz-plane, ——: measured E_ϕ, − − −: measured E_θ, $\cdots\circ\cdots$: simulated E_ϕ, $-\cdot\times-\cdot$: simulated E_θ, all parameters are the same as in Fig. 9.

on the xz-plane is roughly elliptical in shape, with variations within 5 dB.

Fig. 12 shows the radiation patterns at 5.2 and 5.8 GHz, respectively, with corresponding antenna gains of 2.37 and 3.7 dB, respectively. The measured antenna gain averaged over 5.15–5.85 GHz is about 3.2 dBi. The main beam points toward the y-direction. On the yz-plane, the HPBW is about 85° with the third-harmonic mode of the strip monopole, and is about 90° with the second resonant mode of the slot. Different shapes of radiation patterns are consistent with different resonant modes at different bands, as discussed in the previous section.

For practical applications where the users tend to hold their devices in different positions and gestures, the total efficiency $e_o = e_{cd}(1 - |S_{11}|^2)$ could be another parameter to describe the antenna performance, where e_{cd} stands for antenna radiation efficiency.

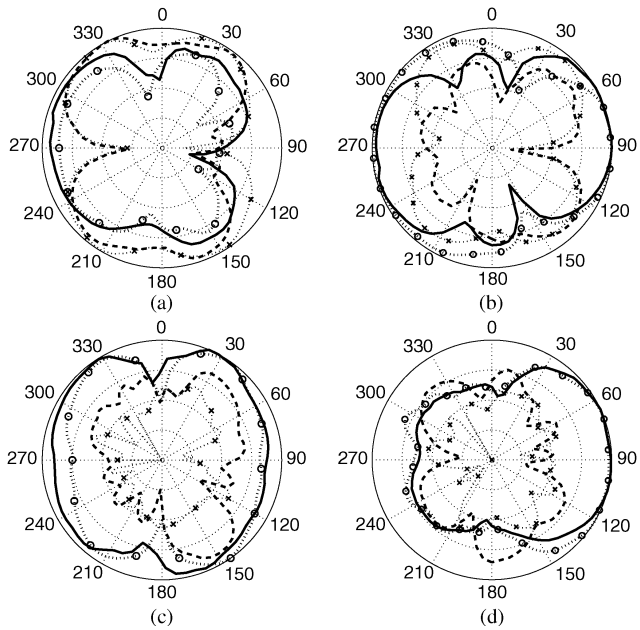

Fig. 12. Radiation patterns, (a) xz-plane at 5.2 GHz, (b) yz-plane at 5.2 GHz, (c) xz-plane at 5.8 GHz, (d) yz-plane at 5.8 GHz, ——: measured E_ϕ, − − −: measured E_θ, $\cdots\circ\cdots$: simulated E_ϕ, $-\cdot\times-\cdot$: simulated E_θ, all parameters are the same as in Fig. 9.

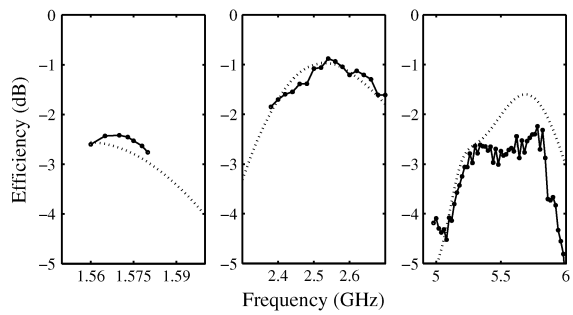

Fig. 13. Total efficiency, all parameters are the same as in Fig. 9, $-\circ-$: measurement, $\cdots$: simulation.

TABLE I
AVERAGE TOTAL EFFICIENCY AND PEAK GAIN

	Total efficiency (dB)			
Frequency (GHz)	1.555-1.5775	2.395-2.695	4.975-5.935	
Average	−2.50	−1.3	−3.13	
Highest	−2.42	−0.88	−2.2	
Lowest	−2.76	−1.7	−4.5	
Frequency (GHz)	1.565	2.62	5.3	5.85
Peak gain (dBi)	0.26	4.36	3.7	4.3

Fig. 13 shows the total efficiency over different bands. The total efficiency is −2.5 dB (56%) at 1.575 GHz, and the average total efficiency over the operating band of 2.4-2.485 GHz is −1.5 dB (70%), both match the simulation results well. The measured total efficiency averaged over the operating band of 5.15–5.85 GHz is −2.8 dB (52%), about 0.7 dB deviated from the simulation. The difference is more significant at higher frequencies, which may be attributed to the loss in the connectors, the twisted cables, and measurement tolerance. Small ripples around 5.2-5.8 GHz may be attributed to the calibration error. Table I lists the peak gain and the total efficiencies, including

the average, the highest, and the lowest, respectively, over the 10-dB impedance bandwidth corresponding to each resonant mode. The simulation shows that the total efficiency of the fundamental slot mode can be slightly improved by about 0.4 dB when e is increased from 1.5 to 5.5 mm, while that of the third-harmonic of the strip monopole mode is decreased by about 0.8 dB.

This slot antenna can be embedded on PCB of a notebook PC or a tablet, or on the metal casing of a handheld device.

VI. Conclusion

A multi-band H-shaped slot antenna has been designed, with a complete analysis on its geometrical parameters. Its 10-dB impedance bandwidth covers the bands of 1.555–1.5775 GHz, 2.395–2.695 GHz and 4.975–5.935 GHz, making it ready for GPS and Wi-Fi applications. Four different operating resonant modes are identified, and the effects of different parameters on these modes have also been analyzed for consistency. Radiation patterns and total radiation efficiency are also presented, and the measurements confirm the simulation results reasonably well.

References

[1] S. K. Sharma, L. Shafai, and N. Jacob, "Investigation of wide-band microstrip slot antenna," *IEEE Trans. Antennas Propag.*, vol. 52, no. 3, pp. 865–872, Mar. 2004.

[2] S.-W. Qu, J.-L. Li, J.-X. Chen, and Q. Xue, "Ultrawideband strip-loaded circular slot antenna with improved radiation patterns," *IEEE Trans. Antennas Propag.*, vol. 55, no. 11, pp. 3348–3353, Nov. 2007.

[3] P. Li, J. Liang, and X. Chen, "Study of printed elliptical/circular slot antennas for ultrawideband applications," *IEEE Trans. Antennas Propag.*, vol. 54, no. 6, pp. 1670–1675, Jun. 2006.

[4] W.-S. Chen and F.-M. Hsieh, "Broadband design of the printed triangular slot antenna," in *Proc. IEEE APS Int. Symp.*, Jul. 2004, vol. 4, pp. 3733–3736.

[5] W.-L. Chen, G.-M. Wang, and C. X. Zhang, "Bandwidth enhancement of a microstrip-line-fed printed wide-slot antenna with a fractal-shaped slot," *IEEE Trans. Antennas Propag.*, vol. 57, no. 7, pp. 2176–2179, Jul. 2009.

[6] S. Cheng, P. Hallbjörner, and A. Rydberg, "Printed slot planar inverted cone antenna for ultrawideband applications," *IEEE Antennas Wireless Propag. Lett.*, vol. 7, pp. 18–21, 2008.

[7] Y. F. Liu, K. L. Lau, Q. Xue, and C. H. Chan, "Experimental studies of printed wide-slot antenna for wide-band applications," *IEEE Antennas Wireless Propag. Lett.*, vol. 3, pp. 273–275, 2004.

[8] L. Dang, Z.-Y. Lei, Y.-J. Xie, G.-L. Ning, and J. Fan, "A compact microstrip slot triple-band antenna for WLAN/WiMAX applications," *IEEE Antennas Wireless Propag. Lett.*, vol. 9, pp. 1178–1181, 2010.

[9] P. Liu, Y. Zou, B. Xie, X. Liu, and B. Sun, "Compact CPW-fed tri-band printed antenna with meandering split-ring slot for WLAN/WiMAX applications," *IEEE Antennas Wireless Propag. Lett.*, vol. 11, pp. 1242–1244, 2012.

[10] J.-Y. Jan and J.-W. Su, "Bandwidth enhancement of a printed wide-slot antenna with a rotated slot," *IEEE Trans. Antennas Propag.*, vol. 53, no. 6, pp. 2111–2114, Jun. 2005.

[11] N. Behdad and K. Sarabandi, "A wide-band slot antenna design employing a fictitious short circuit concept," *IEEE Trans. Antennas Propag.*, vol. 53, no. 1, pp. 475–482, Jan. 2005.

[12] J. Y. Sze and K. L. Wong, "Bandwidth enhancement of a microstrip line-fed printed wide-slot antenna," *IEEE Trans. Antennas Propag.*, vol. 49, no. 7, pp. 1020–1024, Jul. 2001.

[13] T. Dissanayake and K. P. Esselle, "UWB performance of compact Lshaped wide slot antennas," *IEEE Trans. Antennas Propag.*, vol. 56, no. 4, pp. 1183–1187, Apr. 2008.

[14] J.-Y. Jan and L.-C. Wang, "Printed wideband Rhombus slot antenna with a pair of parasitics strips for multiband applications," *IEEE Trans. Antennas Propag.*, vol. 57, no. 4, pp. 1267–1270, Apr. 2009.

[15] S. H. Lee, Y. Lim, Y. J. Yoon, C.-B. Hong, and H.-I. Kim, "Multiband folded slot antenna with reduced hand effect for handsets," *IEEE Antennas Wireless Propag. Lett.*, vol. 9, pp. 674–677, 2010.

[16] C.-I. Lin and K.-L. Wong, "Printed monopole slot antenna for internal multiband mobile phone antenna," *IEEE Trans. Antennas Propag.*, vol. 55, no. 12, pp. 3690–3697, Dec. 2007.

[17] Y. Cao, B. Yuan, and G. Wang, "A compact multiband open-ended slot antenna for mobile handsets," *IEEE Antennas Wireless Propag. Lett.*, vol. 10, pp. 911–914, 2011.

[18] K.-L. Wong and L.-C. Lee, "Multiband printed monopole slot antenna for WWAN operation in the laptop computer," *IEEE Trans. Antennas Propag.*, vol. 57, no. 2, pp. 324–330, Feb. 2009.

[19] J.-S. Chen, "Studies of CPW-fed equilateral triangular-ring slot antennas and triangular-ring slot coupled patch antennas," *IEEE Trans. Antennas Propag.*, vol. 53, no. 7, pp. 2208–2211, Jul. 2005.

[20] N. Behdad and K. Sarabandi, "A varactor dual-band slot antenna," *IEEE Trans. Antennas Propag.*, vol. 54, no. 2, pp. 401–408, Feb. 2006.

[21] S.-Y. Chen, Y.-C. Chen, and P. Hsu, "CPW-fed aperture-coupled slot dipole antenna for tri-band operation," *IEEE Antennas Wireless Propag. Lett.*, vol. 7, pp. 535–537, 2008.

A Compact Dual-Polarized Double E-Shaped Patch Antenna With High Isolation

Yanshan Gou, Shiwen Yang, Quanjiang Zhu, and Zaiping Nie

***Abstract*—A compact dual-polarized double E-shaped patch antenna with high isolation for pico base station applications is presented in this communication. The proposed antenna employs a stacked configuration composed of two layers of substrate. Two modified E-shaped patches are printed orthogonally on both sides of the upper substrate. Two probes are used to excite the E-shaped patches, and each probe is connected to one patch separately. A circular patch is printed on the lower substrate to broaden the impedance bandwidth. Both simulated and measured results show that the proposed antenna has a port isolation higher than 30 dB over the frequency band of 2.5 GHz – 2.7 GHz, while the return loss is less than −15 dB within the band. Moreover, stable radiation pattern with a peak gain of 6.8 dBi – 7.4 dBi is obtained within the band.**

***Index Terms*—Dual-polarization, E-shaped patch, high isolation, microstrip antenna.**

I. Introduction

With the development of base station for next generation mobile communication, compact microstrip antennas have received much attention for their attractive features, such as light weight, low profile, low cost, and ease to integrate with circuits. These features of microstrip antenna attracted amounts of researchers to study and a series of literatures have been reported [1]–[5]. Dual-polarized antenna is commonly used to improve the system performance by polarization diversity in base station. In a dual-polarized antenna with both transmitting and receiving channels for a frequency-reuse communica-

Manuscript received September 21, 2012; revised March 26, 2013; accepted May 01, 2013. Date of publication May 13, 2013; date of current version July 31, 2013. This work was supported in part by the Natural Science Foundation of China (Grant no. 61125104 and 61231001), the 111 project of China (Grant No. B07046) and in part by the Program for Innovation Team in University (No. IRT1113).

The authors are with the School of Electronic Engineering, University of Electronic Science and Technology of China (UESTC), Chengdu 611731, China (e-mail: swnyang@ uestc.edu.cn).

Color versions of one or more of the figures in this communication are available online at http://ieeexplore.ieee.org.

Digital Object Identifier 10.1109/TAP.2013.2262664